EPR Characterization of the Light-Induced Negative Polaron in a Functionalized Dithienylthiazolo[5,4-d]thiazole Acceptor for Organic Photovoltaics

DOI: 10.1007/s00723-019-01146-4
Handle: http://hdl.handle.net/1942/30351

EPR characterization of the light-induced negative polaron in a functionalized dithienylthiazolo[5,4-*d*]thiazole acceptor for organic photovoltaics

Melissa Van Landeghem[a], Julija Kudrjasova[b,c], Wouter Maes[b,c], Etienne Goovaerts[a], Sabine Van Doorslaer[a]*

(a) Experimental Condensed Matter Physics, Physics Department, University of Antwerp, Universiteitsplein 1, B-2610 Antwerpen, Belgium
(b) Design & Synthesis of Organic Semiconductors (DSOS), Institute for Materials Research (IMO-IMOMEC), Hasselt University, Agoralaan 1, B-3590 Diepenbeek, Belgium
(c) Imec, Associated Laboratory IMOMEC, Wetenschapspark 1, B-3590 Diepenbeek, Belgium

Corresponding author: E-mail: sabine.vandoorslaer@uantwerpen.be

Abstract

Functionalized 2,5-dithienylthiazolo[5,4-*d*]thiazole (DTTzTz) derivatives have attracted interest for application as non-fullerene acceptors in solution-processed organic solar cells. Here, we present a combined high-field EPR and DFT study of the light-induced negative polaron on the novel acceptor 2,4-diCN-Ph-DTTzTz formed after charge transfer in bulk heterojunction blends with a donor polymer. Despite spectral overlap with the polymer cation, the ***g***-anisotropy of the acceptor radical could be directly confirmed through detection of its unique ^{14}N hyperfine couplings using electron-electron double resonance (ELDOR)-detected NMR (EDNMR) for spectral filtering. The spectral assignment is further underpinned by quantum-chemical calculations, which also provide detailed information about the spin density and charge distribution of the polaron in the DTTzTz acceptor.

Acknowledgments

The authors want to acknowledge the Research Foundation Flanders (FWO - Vlaanderen) for support of this work through the project G0B6715N and the PhD fellowship of M. Van Landeghem.

1. Introduction

With record power conversion efficiencies (PCEs) in the lab now surpassing the 15% [1] threshold considered as the lower limit for commercial applications, organic solar cells (OSCs) are close to realizing their potential as a promising photovoltaic technology. For decades, high-performing OSCs relied on a junction between a donor polymer and a fullerene acceptor like phenyl-C_{61}-butyric acid methyl ester (PCBM) for charge generation from the strongly bound excitons created upon illumination. Yet, in recent years, the poor absorption properties, limited chemical tunability and high production cost of fullerenes have driven the development of novel non-fullerene acceptors which are now even outperforming the best polymer-fullerene systems, both in terms of PCE [1,2] and stability of the cells [3]. As demonstrated earlier, the 2,5-dithienylthiazolo[5,4-*d*]thiazole (DTTzTz) structural motif exhibits some excellent characteristics towards application in organic photovoltaics: a high stability towards oxidation [4] and strong planarity of the molecular backbone which allows for efficient π-π-stacking and high charge-carrier mobilities in materials based on this unit [5–7]. Moreover, depending on the functionalization pattern, the energy levels of the frontier orbitals can be tuned such that the resulting molecules can act either as donor or as acceptor in combination with other OSC materials [8,9]. The non-fullerene 2,4-diCN-Ph-DTTzTz acceptor studied in this work is the strongest electron acceptor in a series of four similar functionalized DTTzTz derivatives, whose molecular structures and band diagram with highest occupied molecular orbital (HOMO) and lowest unoccupied molecular orbital (LUMO) levels are shown in Figure 1. When combined with donor polymer poly[2-methoxy-5-(3',7'-dimethyloctyloxy)-1,4-phenylene vinylene] (MDMO-PPV), all of the DTTzTz derivatives in Figure 1 are expected to form a type-II band alignment with the polymer and would therefore make suitable electron acceptors. Yet, despite observations of efficient charge transfer (CT), device performance in solar cells based on bulk heterojunction (BHJ) blends of MDMO-PPV and the aforementioned DTTzTz-based acceptors was particularly poor, with PCEs below 0.1% [10,11].

The desired result of the CT process in BHJ OSCs is the formation of a pair of spatially-separated charges: a hole or positive polaron in the donor region and a negative polaron in the nearby acceptor domain. Electron paramagnetic resonance (EPR) methods are particularly useful to study CT and charge generation in OSC blends, because of their selectiveness in probing the positive and negative polarons in the blend [12]. Similar *g*-values are nevertheless expected for these two organic radicals created after CT and spectral overlap therefore often complicates the unambiguous assignment of the light-induced (LI-) EPR spectrum. A previous high-field EPR study [13] by some of the authors on chemically-induced radicals in Th-DTTzTz and 4-CN-Ph-DTTzTz (Figure 1) demonstrated that positive and negative DTTzTz polarons can be distinguished based on their respective principal *g*-values. Although a full ***g***-tensor characterization of the 4-CN-Ph-DTTzTz anion could be obtained, slight differences are still to be expected between such polarons obtained by chemical doping and the light-induced polarons generated by CT in an actual OSC blend. An illustrative case is the light-induced positive polaron in polythiophene, which was found to be more delocalized over the polymer chain than when generated by chemical doping, most likely due to the absence of any counter ions from the oxidizing agent [14]. Yet, in LI-EPR experiments on BHJ blends of Th-DTTzTz, 4-CF_3-Ph-DTTzTz and 4-CN-Ph-DTTzTz with MDMO-PPV, the negative DTTzTz radicals could hardly be observed [10]. Successful CT was, however, demonstrated indirectly by the clear presence of the polymer polaron signal in the LI-EPR spectrum of the blends. In these systems, the driving force for CT was limited by the relatively small LUMO offset between donor and acceptor. In line with the

trend of decreasing LUMO levels within this series of acceptors (Figure 1), the strongest intensity of the polaron signal was found for the blend with 4-CN-Ph-DTTzTz. Yet, even for 4-CN-Ph-DTTzTz, only a very weak signature appeared in the LI-EPR spectrum that was tentatively attributed to the acceptor anion [10]. Moreover, the weak signal was partly overlapping with the polymer cation contribution, further hindering the spectral analysis. A detailed characterization of the light-induced polaron states can, however, give valuable insight into their electronic structure and spatial extent throughout the molecular structure.

In this work we use a combination of high-field EPR and density functional theory (DFT) calculations to fully characterize the negative 1,4-diCN-Ph-DTTzTz polaron. Being the strongest electron acceptor in a series of functionalized DTTzTz derivatives, this is the first DTTzTz acceptor for which the negative polaron could be probed directly and in detail via LI-EPR in donor:acceptor blends with MDMO-PPV.

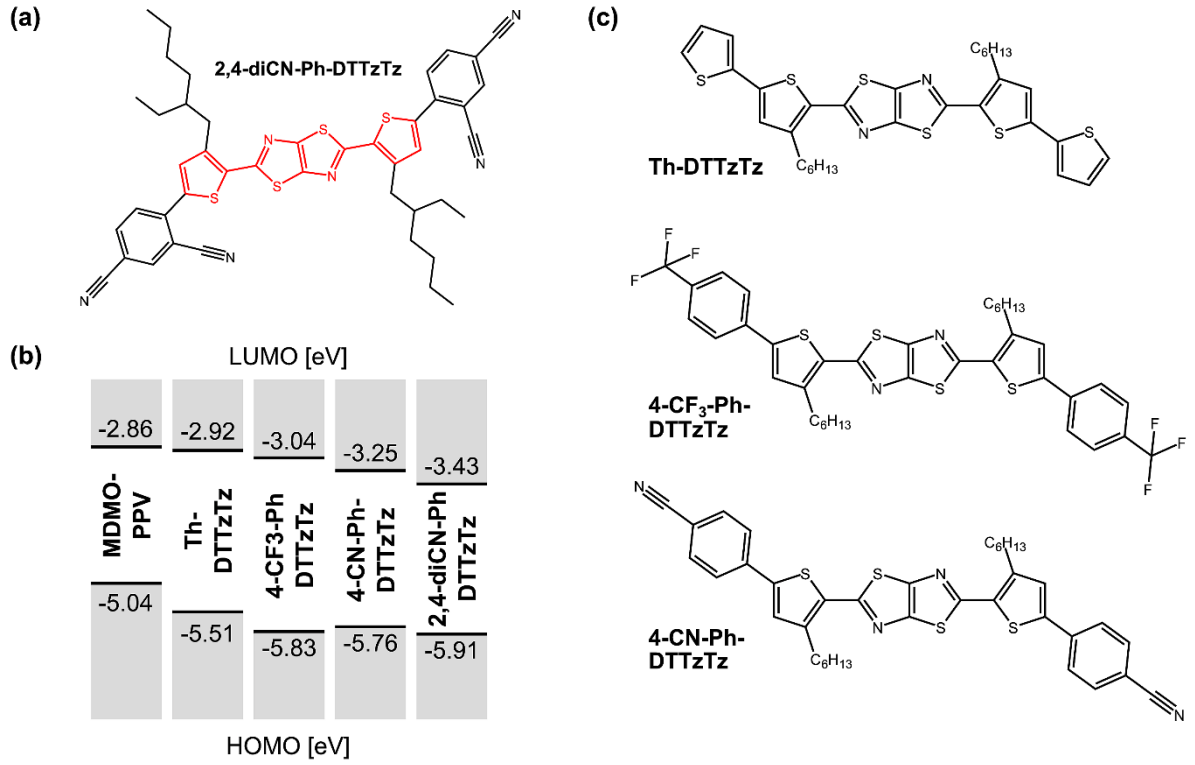

Fig. 1 (a) Chemical structure of the 2,4-diCN-Ph-DTTzTz acceptor studied in this work. The DTTzTz unit is highlighted in red. (b) Band diagram of the materials under study and the related DTTzTz derivatives reported earlier as acceptors in OSCs with MDMO-PPV [10]. The HOMO/LUMO levels were taken from [8,10], where they were derived from cyclic voltammetry in solution. (c) Chemical structures of the Th-DTTzTz, 4-CF_3-Ph-DTTzTz and 4-CN-Ph-DTTzTz derivatives.

2. Materials and methods

Sample preparation

The small molecular acceptor was synthesized following a direct arylation approach as described in [8,11]. Donor polymer MDMO-PPV was purchased from Sigma-Aldrich (M_w~120 000) and used as-received. EPR samples were prepared by scratching off drop-cast films dried on a glass substrate and

transferring the collected material into a quartz sample tube of appropriate size for W-band EPR (I.D. 0.6 mm, O.D. 0.84 mm). The blend film was drop-cast from a chloroform solution prepared with a 1:1 donor:acceptor weight ratio, amounting to a total weight over solvent volume of 10 mg/ml. The pure donor and acceptor films were drop-cast from 10 mg/ml solutions in chlorobenzene.

Magnetic resonance spectroscopy

A Bruker Elexsys E680 W-band spectrometer was used for high-field EPR. It is equipped with a standard single-mode cylindrical resonator from Bruker and a continuous-flow cryostat and superconducting magnet from Oxford Instruments. To allow for light-induced experiments, the sample was illuminated with the second-harmonic output of a CW Nd:YAG laser (λ=532 nm) via a fused silica optical fiber (core diameter: 600 µm), into the quartz sample tube acting as a light guide (20 mW laser power at the end of the fiber). This photon energy is well within the absorption range of both donor and acceptor compounds [8]. Field-swept W-band spectra were recorded by electron spin echo (ESE) detection using the pulse sequence $\pi/2$-τ-π-τ-echo with $t_{\pi/2}$=120 ns, inter-pulse delay τ=400 ns and two-step phase-cycling. All experiments were performed at 80 K and with a shot repetition rate of 200 Hz. The LI ESE-detected EPR spectra are presented as difference spectra (light-minus-dark) in order to determine the light-induced components. The original light and dark spectra can be found in the SI. To account for small frequency differences between measurements, all of the presented spectra were scaled to the same mw frequency (94.04 GHz).

EDNMR was performed under illumination using the pulse sequence t_{HTA}-t_d- $\pi/2$-τ-π-τ-echo. The high-turning angle (HTA) microwave (mw) pulse was applied at frequency ν_1. After a delay time t_d=4µs, it is followed by an echo detection sequence at fixed frequency ν_0, which is on resonance with an EPR transition at the applied magnetic field. The length of the HTA pulse was optimized to t_{HAT}=14 µs; the pulse lengths and inter-pulse delay τ in the ESE detection sequence were the same as in the field-swept EPR experiments and the echo integration window was set to 300 ns. The EDNMR spectrum was then obtained by sweeping the HTA pulse frequency ν_1 over a 50 MHz range about the resonant mw frequency ν_0 of the spin echo detection sequence. The mw field amplitude of the HTA pulse is fixed in this set-up to $\omega_1/2\pi$=2.0 MHz. EDNMR-induced EPR for spectral filtering was performed by recording the EPR spectrum twice using the EDNMR pulse sequence with fixed HTA pulse frequency: once with the mw offset ($\Delta\nu=\nu_1-\nu_0$) fixed on-resonance with the ^{14}N nuclear frequencies (Δν=10MHz) and once with Δν off-resonance (Δν=25MHz). The EDNMR-induced EPR spectrum is then obtained by subtracting the two traces. No phase-cycle was used in the EDNMR experiments.

The simulations of the EPR spectra were performed with the Easyspin software package (version 5.1.3) [15].

Computational methods

Spin-unrestricted DFT calculations were performed with the ORCA quantum chemistry package (version 2.9.1) [16–18]. The molecular geometry was first optimized using the BP86 functional [19] and the SVP basis set [20] for all atoms. Single-point calculations of the EPR parameters were performed using the hybrid B3LYP functional [19,21] combined with the EPR-II basis set [22] for the light elements and the TZV-PP basis set [20] for S. All calculations were performed in vacuo. All calculations were repeated for three conformations of the 2,4-diCN-Ph-DTTzTz molecular structure.

3. Results and discussion

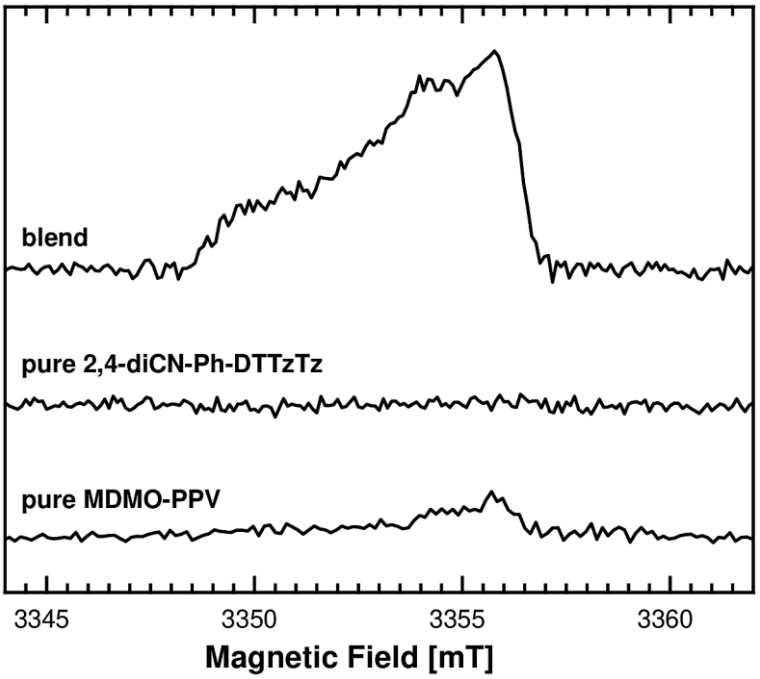

Fig. 2 W-band LI-EPR spectra of the 1:1 MDMO-PPV:2,4-diCN-Ph-DTTzTz blend and the pure donor and acceptor control samples.

In the earlier LI-EPR study of the BHJ blends of Th-DTTzTz, 4-CF_3-Ph-DTTzTz and 4-CN-Ph-DTTzTz with MDMO-PPV only a single resonance line was observed in the X-band spectra [10]. Hence, to resolve the two-component character expected for a pair of CT radicals, all EPR experiments on the MDMO-PPV:2,4-diCN-Ph-DTTzTz were performed at W-band frequency. Figure 2 shows the light-induced W-band spectra of the 1:1 MDMO-PPV:2,4-diCN-Ph-DTTzTz blend and the pure donor and acceptor samples. The original dark spectra are included in the SI. Before illumination, a weak signal was present in the blend EPR spectrum, increasing significantly when the light was switched on. Moreover, the (near-)absence of light-induced components in the pure donor and acceptor samples confirms that the blend EPR signal originates from CT radicals. Overall, the signal intensity is rather weak, suggesting a low charge generation yield in the blend, which correlates well with the poor PCEs observed in OSC devices based on this donor-acceptor combination [11].

Although the EPR spectrum seems to consist of two different organic radical contributions, the individual components are poorly resolved even at W-band frequency. Fortunately, workhorse donor polymer MDMO-PPV has been intensively studied and reference data for the ***g***-tensor of the MDMO-PPV^+ polaron are readily available [23]. As such, the principal *g*-values of the acceptor anion could be obtained by simultaneous fitting of the blend EPR spectrum as shown in Figure 3. The principal *g*-values of the CT radicals used for the simulations in Figure 3 are summarized in Table 1. Although some uncertainty remains for the g_x-component of the 2,4-diCN-Ph-DTTzTz anion due to spectral overlap with MDMO-PPV^+, the simultaneous fitting allowed for a determination of the ***g***-tensors of the two CT radicals. For the MDMO-PPV polaron, a good agreement with the literature data was obtained [23].

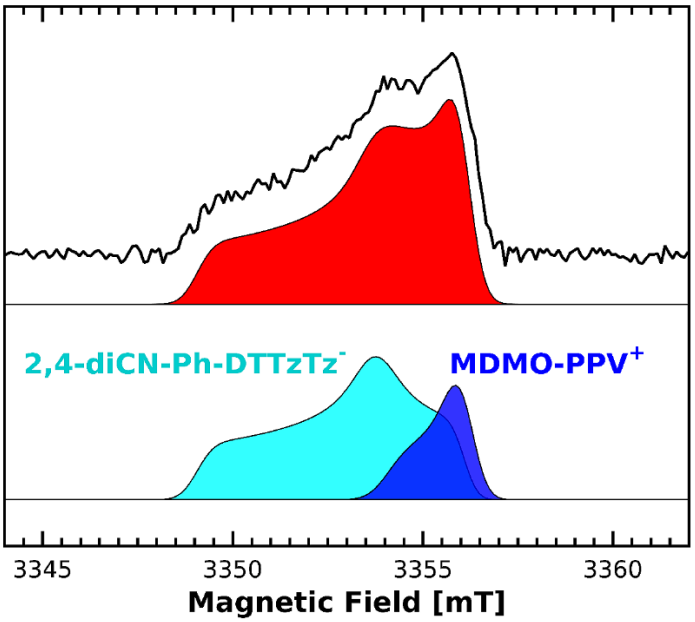

Fig. 3 W-band LI-EPR spectrum of the 1:1 MDMO-PPV:2,4-diCN-Ph-DTTzTz blend (black) and simulation of the positive polaron P^+ on the polymer and the negative polaron P^- on the acceptor molecule in blue and cyan, respectively. Red: sum of the two simulations. The principal *g*-values used in the simulations are given in Table 1.

Table 1 Comparison of the experimental *g*-values obtained by simulation of the W-band EPR spectrum shown in Fig. 3 and the DFT-computed *g*-values for both oxidation states of the 2,4-diCN-Ph-DTTzTz radical. The estimated error in the experimental *g*-values is ±0.0001. For the polaron on MDMO-PPV, a comparison with the experimental *g*-values obtained in [23] is made.

	Positive polaron			Negative polaron			
	g_x	g_y	g_z	g_x	g_y	g_z	Method
diCN-DTTzTz	n.d.	n.d.	n.d.	2.0021	2.0035	2.0063	Exp.
	2.0006	2.0022	2.0031	2.0024	2.0046	2.0072	DFT
MDMO-PPV	2.0021	2.0021	2.0033	n.d.	n.d.	n.d.	Exp.
	2.0022	2.0022	2.0033				Exp. [23]

To confirm the determination of the 2,4-diCN-Ph-DTTzTz$^-$ ***g***-tensor, electron-electron double resonance (ELDOR)-detected NMR (EDNMR) was used to explicitly map the EPR contribution of the acceptor radical in the region of overlap with the polymer polaron by probing its hyperfine couplings to the ^{14}N nuclei in the 2,4-diCN-Ph-DTTzTz backbone. The EDNMR spectrum of the MDMO-PPV:2,4-diCN-Ph-DTTzTz blend was recorded at two different field positions: at B=3350.6 mT, where the EPR signal would originate solely from 2,4-diCN-Ph-DTTzTz$^-$, and at B=3356.0 mT, where the spectra of both MDMO-PPV$^+$ and 2,4-diCN-Ph-DTTzTz$^-$ overlap. When $\Delta\nu$=0, the EPR transition becomes nearly saturated. As a result, the EDNMR spectrum exhibits a central blindspot with a Lorentzian lineshape, which is a common feature of EDNMR experiments. This is illustrated in Figure 4(a), which shows the EDNMR spectrum of the blend recorded at B=3356.0 mT, before subtraction of this Lorentzian background. Figure 4(b) shows the same spectrum after background correction, together with the EDNMR spectrum recorded at the low-field side of the LI-EPR spectrum. Since there are no nitrogen

nuclei in the polymer structure, we can directly relate the presence of ^{14}N couplings in the EDNMR spectrum to an acceptor radical contribution to the total EPR signal at that field position. For weakly coupled nuclei, the EDNMR signal is expected to be centered around their respective Larmor frequency, which is about 10 MHz for ^{14}N at typical W-band magnetic field strengths. The width of the EDNMR peak will in turn be determined by the hyperfine and quadrupole coupling strength. In both EDNMR spectra, we indeed find a rather broad signature at Δν=10 MHz stemming from ^{14}N couplings. Regardless of the spectral overlap with the MDMO-PPV^{+} signature, the contribution of the 2,4-diCN-Ph-DTTzTz radical at the high-field side of the spectrum is hereby unambiguously demonstrated. Hence the predicted ***g***-anisotropy of the acceptor radical, extending over the entire width of the EPR spectrum, is directly confirmed.

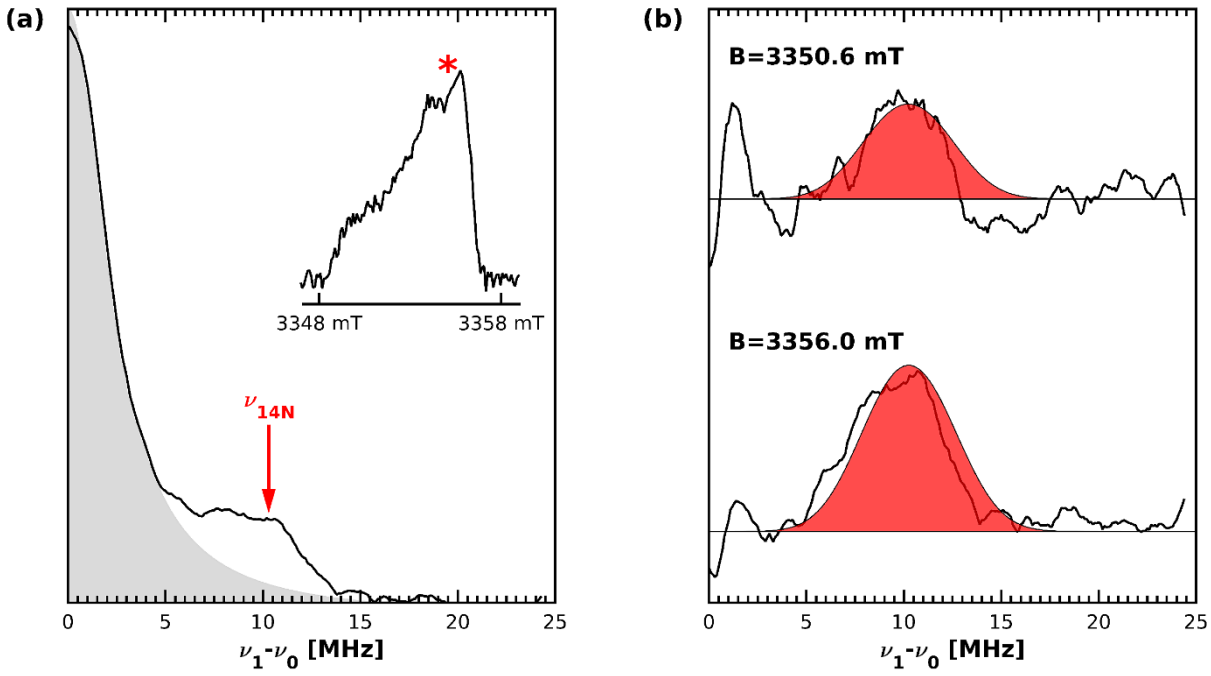

Fig. 4 (a) W-band EDNMR spectrum of MDMO-PPV:2,4-diCN-Ph-DTTzTz recorded at *B*=3356.0 mT, before subtraction of the central Lorentzian blindspot at Δν=0 MHz. The magnetic field position at which the EDNMR spectrum is recorded, is indicated by a red asterisk in the EPR spectrum in the inset. A fit of the central Lorentzian is shown in gray. ν_{14N} indicates the Larmor frequency of ^{14}N at the applied magnetic field strengths. (b) W-band EDNMR spectrum of MDMO-PPV:2,4-diCN-Ph-DTTzTz recorded at *B*=3350.6 mT (top) and *B*=3356.0 mT (bottom), after subtraction of the fit of the Lorentzian background (black). Red: Simulations of the EDNMR spectra based on the DFT-computed ^{14}N hyperfine and quadrupole tensors of the 2,4-diCN-Ph-DTTzTz anion given in Table 2. A linewidth of 4MHz (full width at half maximum) was used for the simulation.

The EDNMR linewidth is mainly determined by the length of the echo integration window, as demonstrated by the empirical relation derived in [24]. As such, the resolution of the EDNMR spectra shown in Figure 4 is limited to about 4.7 MHz because of the short echo integration window of 300 ns needed for a workable signal-to-noise ratio. This is larger than the maximal hyperfine splittings expected according to the DFT-computed hyperfine and quadrupolar parameters for the 2,4-diCN-Ph-DTTzTz^{-} radical (see Table 2 below). As a result, the EDNMR peak of the ^{14}N couplings exhibits very little substructure due to orientational selection. Under these conditions, we can assume that the

EDNMR peak intensity is proportional to the contribution of the 2,4-diCN-Ph-DTTzTz radical to the total echo at each field position. As such, one can directly filter out the EPR spectrum of the 2,4-diCN-Ph-DTTzTz radical using EDNMR-induced EPR. To this end, the EPR spectrum is recorded with the EDNMR pulse sequence while keeping the frequency offset Δν fixed, once on-resonance with the ^{14}N couplings, once off-resonance. Subtracting these two traces, we obtain a spectrum containing only contributions from the radical coupled to the ^{14}N nuclei. Hence, using EDNMR-induced EPR, we can exploit the presence of the unique ^{14}N couplings of 2,4-diCN-Ph-DTTzTz$^-$ to isolate its contribution to the overlapping EPR spectrum of the blend. The application of EDNMR-induced EPR as a method for spectral filtering of overlapping high-field EPR spectra has recently been demonstrated for the first time in another fullerene-free OSC blend [25].

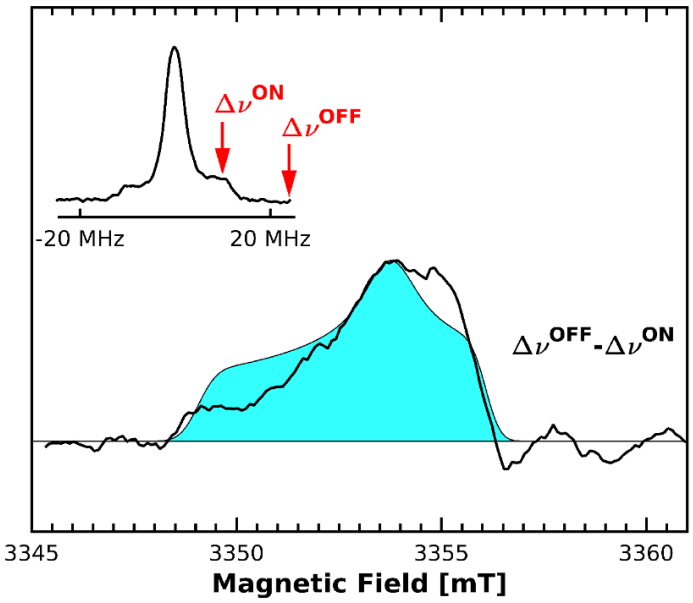

Fig. 5 W-band EDNMR-induced EPR spectrum of MDMO-PPV:2,4-diCN-Ph-DTTzTz, obtained by subtracting the field-swept spectra recorded with HTA pulse frequency offsets $\Delta\nu^{OFF}$=25 MHz and $\Delta\nu^{ON}$=10 MHz. The position of the mw frequency offsets in the *B*=3356.0 mT EDNMR spectrum are shown in the inset. The simulation based on the 2,4-diCN-Ph-DTTzTz$^-$ *g*-values obtained from fitting the EPR spectrum in Fig. 3 is shown in cyan.

Figure 5 shows the EDNMR-induced EPR spectrum obtained for the 2,4-diCN-Ph-DTTzTz anion by subtracting the field-swept spectra recorded with HTA pulse frequency offsets $\Delta\nu^{OFF}$=25 MHz and $\Delta\nu^{ON}$=10 MHz. In spite of the low signal-to-noise level, the EDNMR-induced EPR spectrum is found to agree well with the simulation of the 2,4-diCN-Ph-DTTzTz anion obtained earlier by fitting the LI-EPR spectrum in Figure 3. Hence the EDNMR-induced EPR spectrum confirms the expected ***g***-anisotropy of the acceptor radical and corroborates the principal *g*-values assigned to 2,4-diCN-Ph-DTTzTz$^-$, in particular g_x, given in Table 1.

In order to underpin the magnetic resonance parameters obtained experimentally, we performed DFT computations of the electronic ***g***-tensor of the 2,4-diCN-Ph-DTTzTz acceptor radical. A previous EPR study on DTTzTz derivatives established that these derivatives can act either as donor or as acceptor, depending on the chemical functionalization [13]. Moreover, the ***g***-tensor of the corresponding radicals was found to depend more strongly on the oxidation state than on the differences in chemical structure. Hence, in order to validate our assignment of the EPR spectrum in

Figure 3 to negatively charged polarons on 2,4-diCN-Ph-DTTzTz, we calculated the ***g***-tensor for both (singly-charged) oxidation states of the molecule. Depending on the *cis/trans* configuration of the outer thiophene units, three different conformers of the 2,4-diCN-Ph-DTTzTz molecule exist (see Figure SI.2) and ***g***-tensor calculations were performed for each of them. The negative radical states of the different conformers were found to be near iso-energetic, although these relative energy differences should be interpreted with care as the calculation does not account for the non-vacuo surroundings and steric effects in an actual blend film. The DFT-computed *g*-values for the ground-state conformer of 2,4-diCN-Ph-DTTzTz are summarized in Table 1 to allow for direct comparison with the experimental parameters obtained via simulation of the blend spectrum. The *g*-values computed for the other conformations are included in the SI. Because, for a given oxidation state, very similar *g*-values were obtained for all configurations, co-existence of the different conformers in the sample would not lead to significant ***g***-strain broadening.

Despite a slightly larger ***g***-anisotropy and a somewhat overestimated g_{iso}, the theoretically predicted *g*-values for the negative 2,4-diCN-Ph-DTTzTz radical are indeed in good agreement with those obtained experimentally. Qualitatively the same trends are obtained: one g-value (g_x) is nearly equal to the free electron *g*; the other *g*-values are both larger than g_e. The deviations between the computed and experimental *g*-values of at most 0.0012 are within the accuracy expected for this type of calculations. DFT furthermore provides the orientation of the ***g***-tensor principal axes system with respect to the molecular axes, which cannot be determined experimentally from a powder EPR spectrum. As such we find that g_x has its principal axis pointing out of the molecular plane, which explains the small deviation from g_e. The axes of g_y and g_z are both lying within the conjugation plane, respectively perpendicular and parallel to the molecular backbone. The *g*-values computed for the positive 2,4-diCN-Ph-DTTzTz radical on the other hand do not even qualitatively reproduce the experimentally observed trends, since one of the *g*-values is significantly smaller than g_e. Hence, the DFT calculations support our earlier assignment of the EPR spectrum and confirm that 2,4-diCN-Ph-DTTzTz indeed acts as an acceptor in combination with MDMO-PPV.

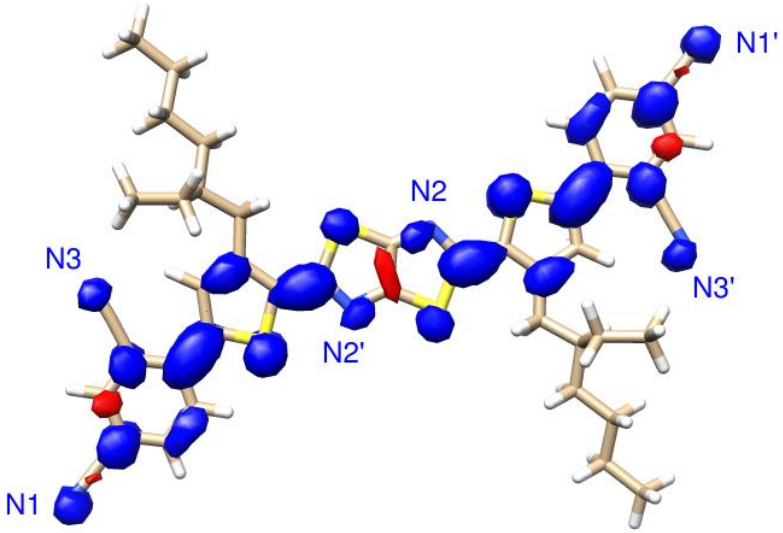

Fig. 6 Spin density distribution of the negative radical state of the ground-state 2,4-diCN-Ph-DTTzTz conformer based on DFT calculations. Red: Negative spin density. Blue: Positive spin density. Contour levels were fixed at -0.001 and 0.001, respectively.

As the ***g***-tensor is a global probe of the electronic structure, it cannot be straightforwardly interpreted in terms of the spatial delocalization of the polaron along the molecular structure. Yet, the supporting DFT computations do provide a microscopic picture of the spin density distribution of the polaron states. Figure 6 shows a contour plot of the spin density of the ground state conformer of 2,4-diCN-Ph-DTTzTz^{-}. The spin density contour plots of the positive radical state of this conformer and of both oxidation states of the two higher-energy 2,4-diCN-Ph-DTTzTz conformers are included in the SI. For each oxidation state, similar spin density distributions were obtained for all conformers. For the negative polarons, the molecular backbone remains planar after geometry optimization. For the positive polarons, the terminal benzodinitrile groups are slightly rotated with respect to the plane determined by the planar DTTzTz backbone (torsion angle of 25°). Both the positive and negative polaron are found to be delocalized over the entire conjugation length of the 2,4-diCN-Ph-DTTzTz backbone with no significant spin density spilling out onto the hexyl side chains.

While the spin density distribution provides insight into the delocalization of the polarons along the 2,4-diCN-Ph-DTTzTz backbone, knowledge of the electronic charge distribution helps to further understand the relative electronegativity of the different functional groups. The total charge on the TzTz core, thiophene rings, benzodinitrile groups and 2-ethylhexyl side chains was derived from Mulliken population analysis by summing up the individual atomic charges corresponding to each molecular fragment. The resulting charge distribution for both the positive and negative radical of all three 2,4-diCN-Ph-DTTzTz conformers is summarized in Table SI.4. As expected, the terminal benzodinitrile groups exhibit the strongest electronegativity compared to the other functional groups. For the anion radical, the benzodinitrile groups alone carry about 60% of the excess negative charge, compared to 25-30% for the central TzTz unit. The thiophene units on the other hand are clearly the strongest electron-donating moiety in the structure and even retain about 0.25 excess positive charge in the anion radical state. Hence, the charge distribution of the 2,4-diCN-Ph-DTTzTz radicals illustrates the push-pull character of this molecule, wherein the thiophene rings act as electron donors and the terminal dicyanophenyl groups and the TzTz core are the electron-withdrawing substituents. The spin density and charge distributions were also calculated for a model system containing both 2,4-diCN-Ph-DTTzTz and a poly(*p*-phenylene vinylene) (PPV) trimer. In the presence of a single negative charge, the spin density was still found to be entirely localized on the DTTzTz acceptor, as expected. Moreover, for the composite system identical *g*-values were obtained as for the individual 2,4-diCN-Ph-DTTzTz molecule (see SI). This result illustrates that the ***g***-tensor of 2,4-diCN-Ph-DTTzTz^{-} is rather insensitive to small structural deformations induced by molecular interactions with the nearby PPV oligomer.

Table 2 DFT-computed ^{14}N hyperfine and quadrupole tensors of the ground-state conformer of the negative 2,4-diCN-Ph-DTTzTz radical.

	A_x [MHz]	A_y [MHz]	A_z [MHz]	α,β,γ [°]	e^2qQ [MHz]	η	α,β,γ [°]
N^1	-0.75	-0.32	4.29	23,88,-4	-3.14	0.34	-5,22,-81
N^2	-0.50	-0.71	1.56	-40,90,1	-3.48	0.33	1,44,89
N^3	-0.24	-0.52	3.08	-3,88,-4	-3.09	0.22	-10,2,14

Table 2 summarizes the calculated ^{14}N hyperfine and quadrupole tensors of the ground state conformer of 2,4-diCN-Ph-DTTzTz^{-}. Since this conformer has a symmetrical molecular structure, the hyperfine and quadrupole couplings of the six nitrogen atoms in the system are two-by-two

equivalent and only one set of inequivalent N atoms is tabulated. The corresponding N nuclei are labelled in Figure 6. For the other conformers similar results were obtained (see SI). Based on the DFT-computed hyperfine and quadrupole couplings, the experimental EDNMR spectra at both field positions could be simulated as shown in Figure 4(b). For the simulations a linewidth of 4 MHz (full width at half maximum) was assumed in accordance with our earlier estimate of the EDNMR spectral resolution from the echo integration time. In the EDNMR spectrum recorded at B=3356.0 mT, the experimental peak position seems to be slightly downshifted with respect to the Larmor frequency of ^{14}N. This deviation could be attributed to the convolution of the EDNMR spectrum with the non-symmetrical resonator bandwidth, which we cannot correct for. Nevertheless, for both EDNMR spectra the width of the ^{14}N feature in the EDNMR spectra is compatible with the DFT-computed hyperfine and quadrupole couplings of the 2,4-diCN-Ph-DTTzTz anion, again confirming its assignment.

Conclusion

In this work we have presented a full characterization of the ***g***-tensor of the light-induced negative polaron in the non-fullerene acceptor 2,4-diCN-Ph-DTTzTz. Being the strongest electron acceptor in a series of related DTTzTz derivatives, this is the first DTTzTz acceptor for which the negative polaron could be directly detected via LI-EPR in an OSC blend with MDMO-PPV. While the spectral overlap with the polymer cation spectrum initially hindered the extraction of the lowest *g*-value, the contribution of the acceptor radical in the overlapping region could be unambiguously demonstrated by probing its unique hyperfine couplings to ^{14}N using EDNMR. The ***g***-tensor assignment was further corroborated by EDNMR-based spectral filtering and supporting DFT calculations.

References:

1. J. Yuan, Y. Zhang, L. Zhou, G. Zhang, H.-L. Yip, T.-K. Lau, X. Lu, C. Zhu, H. Peng, P. A. Johnson, M. Leclerc, Y. Cao, J. Ulanski, Y. Li, and Y. Zou, Joule 1 (2019).

2. J. Hou, O. Inganäs, R. H. Friend, and F. Gao, Nat. Mater. **17**, 119 (2018).

3. W. Zhao, D. Qian, S. Zhang, S. Li, O. Inganäs, F. Gao, and J. Hou, Adv. Mater. **28**, 4734 (2016).

4. I. Osaka, R. Zhang, J. Liu, D.-M. Smilgies, T. Kowalewski, and R. D. McCullough, Chem. Mater. **22**, 4191 (2010).

5. I. Osaka, R. Zhang, G. Sauvè, D. M. Smilgies, T. Kowalewski, and R. D. McCullough, J. Am. Chem. Soc. **131**, 2521 (2009).

6. Naraso and F. Wudl, Macromolecules **41**, 3169 (2008).

7. S. Ando, D. Kumaki, J. I. Nishida, H. Tada, Y. Inoue, S. Tokito, and Y. Yamashita, J. Mater. Chem. **17**, 553 (2007).

8. J. Kudrjasova, R. Herckens, H. Penxten, P. Adriaensens, L. Lutsen, D. Vanderzande, and W. Maes, Org. Biomol. Chem. **12**, 4663 (2014).

9. J. Kudrjasova, M. Van Landeghem, T. Vangerven, J. Kesters, G. H. L. Heintges, I. Cardinaletti, R. Lenaerts, H. Penxten, P. Adriaensens, L. Lutsen, D. Vanderzande, J. Manca, E. Goovaerts, and W. Maes, ChemistrySelect **2**, 1253 (2017).

10. N. Nevil, Y. Ling, S. Van Mierloo, J. Kesters, F. Piersimoni, P. Adriaensens, L. Lutsen, D.

Vanderzande, J. Manca, W. Maes, S. Van Doorslaer, and E. Goovaerts, Phys. Chem. Chem. Phys. **14**, 15774 (2012).

11. M. Van Landeghem, R. Lenaerts, J. Kesters, W. Maes, and E. Goovaerts, (n.d.).

12. J. Niklas and O. G. Poluektov, Adv. Energy Mater. 1602226 (2017).

13. Y. Ling, S. Van Mierloo, A. Schnegg, M. Fehr, P. Adriaensens, L. Lutsen, D. Vanderzande, W. Maes, E. Goovaerts, and S. Van Doorslaer, Phys. Chem. Chem. Phys. **16**, 10032 (2014).

14. J. Niklas, K. L. Mardis, B. P. Banks, G. M. Grooms, A. Sperlich, S. Beaupr, V. Dyakonov, S. Beaupré, M. Leclerc, T. Xu, L. Yu, and O. G. Poluektov, Phys. Chem. Chem. Phys. **15**, 9562 (2013).

15. S. Stoll and A. Schweiger, J. Magn. Reson. **178**, 42 (2006).

16. F. Neese, Wiley Interdiscip. Rev. Comput. Mol. Sci. **2**, 73 (2012).

17. F. Neese, J. Chem. Phys. **115**, 11080 (2001).

18. F. Neese, J. Chem. Phys. **122**, (2005).

19. A. D. Becke, Phys. Rev. A **38**, 3098 (1988).

20. A. Schäfer, H. Horn, and R. Ahlrichs, J. Chem. Phys. **97**, 2571 (1992).

21. C. Lee, W. Yang, and R. G. Parr, Phys. Rev. B **37**, 785 (1988).

22. V. Barone, in *Recent Adv. Density Funct. Methods* (1995), pp. 287–334.

23. A. Aguirre, P. Gast, S. Orlinskii, I. Akimoto, E. J. J. Groenen, H. El-Mkami, E. Goovaerts, and S. Van Doorslaer, Phys. Chem. Chem. Phys. **10**, 7129 (2008).

24. A. Nalepa, K. Möbius, W. Lubitz, and A. Savitsky, J. Magn. Reson. **242**, 203 (2014).

25. M. Van Landeghem, W. Maes, E. Goovaerts, and S. Van Doorslaer, J. Magn. Reson. **288**, 1 (2018).